Turkish Journal of Chemistry

http://journals.tubitak.gov.tr/chem/

Research Article

Turk J Chem
(2021) 45: 485-492
© TÜBİTAK
doi:10.3906/kim-2008-59

Rhenium/rhenium oxide nanoparticles production using femtosecond pulsed laser ablation in liquid

Abdullah KEPCEOĞLU[1], Yasemin GÜNDOĞDU[2,6], Adem SARILMAZ[3], Mustafa ERSÖZ[4,5], Faruk ÖZEL[3], Hamdi Şükür KILIÇ[1,4,6,*]

[1]Department of Physics, Faculty of Science, Selçuk University, Konya, Turkey
[2]Department of Computer Technologies, Kadınhanı Faik İçil Vocational High School, University of Selçuk, Konya, Turkey
[3]Department of Metallurgical and Materials Engineering, Faculty of Engineering, Karamanoğlu Mehmetbey University, Karaman, Turkey
[4]Directorate of High Technology Research and Application Center, Selçuk University, Konya, Turkey
[5]Department of Chemistry, Faculty of Science, Selçuk University, Konya, Turkey
[6]Selçuk University Laser Driven Proton Therapy Research and Application (SULTAN) Center, Konya, Turkey

Received: 31.08.2020 • **Accepted/Published Online:** 25.01.2021 • **Final Version:** 28.04.2021

Abstract: In this study, rhenium/rhenium oxide nanoparticles (Re / ReO_3 NPs) have been produced for the first time in ultrapure water by using Femtosecond Pulsed Laser Ablation in Liquid (fsPLAL) method. X-Ray Diffraction (XRD) measurements and results obtained for NPs show the existence of well-crystallized peaks and preferred phases. Re NPs have hexagonal structure while ReO_3 NPs have the perovskite-like cubic crystal structures. The Re / ReO_3 ratio is also determined to be 53 / 47 with ~ 20 nm crystallite size, while pure ReO_3 crystallite sizes were measured to be ~ 25 nm. The TEM results have shown that the produced particles have a spherical shape, and particle sizes changes between ~ 20 nm and ~ 60 nm. The crystallite size is similar due to XRD results. Obtained nanoparticles exhibit promising applications for photonic devices with broad bandgap values which have measured to be 4.71 eV for Re / ReO_3 NPs mixture and 4.36 eV for pure ReO_3 NPs.

Key words: Rhenium nanoparticles, ReO_3, oxide nanoparticles, laser processing, pulsed laser ablation

1. Introduction

Pulsed laser ablation (PLA) of solids is a very promising functional, powerful, and clean method for nanoparticle production [1]. NPs with controlled sizes, shapes, and concentrations can be obtained using PLA. PLA in liquid (PLAL) method becomes a facile and clean (free of contaminats) method to produce NPs [2] because this method can easily be used to produce NPs in a reservoir of ultrapure water, water surfactant mixtures or some other liquid materials [3]. Metallic NPs may have very broad area of applications as such copper [4] and silver [5] could be used as an antibacterial potency against *E. coli*. Especially, gold NPs were extensively used in very broad application area including catalysis, nanotechnology [6], cancer diagnostics [7], and biological applications [8]. Also, Au NPs are widely used in thin film applications [9,10] and in nonvolatile memory devices [11].

In recent years, rhenium nanoparticles (NPs) have been used in several applications such as a tumour treating therapies and coating (plastics, metals, textiles) technologies as well as magnetic rhenium NPs, which have been used as a contrast agent and are produced by using chemical or physical methods. Rhenium containing NPs have been studied and reported for catalytic and sensor applications in literature [12,13]; platinum monolayer on iridium/rhenium alloy nanoparticles [14] may function as a core part of some core-shell structures for the oxygen reaction, rhenium-containing Polytetrafluoroethylene (PTFE) structures [15] as catalysts and ReO_3 @ SiO_2, ReO_3 @ Ag, ReO_3 @ Au NPs for sensor applications [16]. There are a few methods reported in the literature for production of Re NPs, which are pulsed laser decomposition [17], reduction of some organometallic complexes [18] or colloidal and microemulsion synthesis in liquid environment [19], but, due to the author's knowledge, no study has yet been reported in the literature about the use of the fsPLAL method for production of Re NPs as well as ReO_3. Rhenium-containing alloys and coatings have been used for high-temperature applications, while Re NPs have also been used to connect parts at lower temperatures [20], which reduces the melting point of alloys. In a recent study, amorphous Re_xO_y NPs were produced in tunable particle sizes

* Correspondence: hamdisukurkilic@selcuk.edu.tr

by using gamma radiation [21]. ReS NPs were synthesized as magnetic nanoparticles [22,23] for the contrast agent. In comparison with other transition metal oxides, ReO_3 has some attractive properties such as having a perovskite-like cubic structure and higher conductivity than metallic rhenium [24]. The resistivity of the single-crystal bulk ReO_3 is about $(8.95 \pm 0.03) \times 10^{-6}\ \Omega\cdot cm$ at 300 K [25]. The optical properties of ReO_3 Nano-Crystals (NCs) were studied by Biswas and Rao [26]. The colloidal ReO_3 NCs exhibits very high enhanced localized surface plasmon resonance (LSPR) in the visible range of spectrum from 488 nm to 534 nm that is comparable to gold NPs LSPR range, and ReO_3 NPs show some metallic behaviours [27]. In a recent study, 8% ReO_3 NPs doped in 1,1-bis-(4-bis(4-methyl-phenyl)-amino-phenyl)-cyclohexane (TAPC) were used as a p-doped hole injection layer (HIL) in transparent organic light emitting diodes (OLED) [28]. Surface plasmon resonance (SPR) nature of ReO_3 NPs has been reported; it has been shown that SPR peaks of NPs lies in the visible range, and it can be tuned over the relevant spectral range by controlling the size of NPs. When particle size tuned from 8.5 nm to 32 nm, SPR peak is also tuned from 490 nm to 540 nm [26]. Recently, researchers are very interested in the production of complex NPs from bulk materials using facile and single step production methods that allow choosing parameters. In this study, the single step facile production of the transition metal/metal oxide (Re / ReO_3) NPs was performed by using fsPLAL method and characterizations together with the interpretation of NPs obtained.

2. Materials and methods

In this work, we have used a Ti:Sapphire femtosecond laser system (Quantronix, Integra-C-3.5, NY, USA) pumped by Kerr-Lens mode-locked Ti:Sapphire laser (Quantronix, Ti-Light, NY, USA) (with 330 mW pulse power). Parameters are given as follow: amplifier laser delivers mode-locked chirped laser pulses with up to 3.5 W per pulse at a wavelength of 810 nm and with 90 fs pulse duration, and 1-3 kHz repetition rate with 8 mm beam diameter. Detailed system parameters were described elsewhere [29].

The laser output was adjusted and controlled by using an oscilloscope (WaveRunner 64 Xi, four channel digital-storage oscilloscope, LeCroy Corporation, NY, USA) triggered with a fast photodiode (Alphalas, UPD-35-UVIR-D, Germany). 0.125 mm thick 99.99% pure rhenium (Goodfellow) target translated to the focal point by using a motorized lab jack (MLJ050, ThorLabs, Newton NJ, USA). We have used micromachining system to scan rhenium target and set laser pulse power to 800mW. Re NPs were produced in ultrapure deionized water (18.3 MΩ·cm) (Millipore, USA) with 1 cm thick water layer above sample ($8.04\ cm^3$).

The experimental setup is shown in Figure 1(a) and PLAL method briefly introduced as depicted in Figure 1(b). In PLAL method, NPs were produced by courtesy of PLAL method from Re plate sinked in liquid applying pulsed fs laser beams. Target located above the target holder when the laser beam enters the water vertically. If laser beam comes horizontal direction, one can use rotating cylindrical or fixed flat surfaced targets. In this work, vertical laser beams were used to ablate target material inside ultrapure water. As a usual case of interaction between fs laser pulses and target, resonance laser ablation (RLA) process is dominated by photoionization processes (single or multiphoton processes) and following locally induced space-charge separation fields and electron-ion collisions cause the formation of cavitation bubble [30]. There is two step in PLAL method, first one is plasma production and the last one is the continued growth of the NPs after collapsing of the plasma [31].

Laser-irradiated $10 \times 10\ mm^2$ surface area of target was put inside the container and 10 mm height ultrapure water added. Marking systems laser input was power reduced to 800 mW, pulses were used at 1 kHz repetition rate and wavelength was 800 nm. Scanning parameters were set to $3\ mm\cdot s^{-1}$ for scanning speed, 250 μm line gap between each scan, working area set to $6 \times 6\ mm^2$ and each line scanned twice.

3. Results and discussion

The crystal structures of Re / ReO_3 nanoparticles produced in this study have been examined using XRD technique (Bruker AXS, Bruker D8 Advance, Germany), and XRD results of powdered NPs are shown in Figure 2.

Figure 2(a) shows XRD spectrum for Re / ReO_3 NPs mixture in a ratio of 53 / 47 produced within 30 min. Diffraction peaks of the produced nanocrystals are intense and neat, showing that the Re NPs have hexagonal (space group: P63 / mmc) structure while ReO_3 NPs have the perovskite-like cubic (space group: Pm-3m) structure [32] with effective crystallization and lack of impurities. The crystallite size of the obtained NPs measured from XRD spectra was calculated using Debye–Scherrer equation, size = $K\lambda/\beta \cos\theta$, where, K is a dimensionless constant, β is full width at half maximum (FWHM in radian), θ is the diffraction Bragg angle and λ is the wavelength of X-ray in equation [33]. The average crystallite size was calculated due the most intense peaks to be 21 nm for ReO_3 and 22 nm for Re using the Debye-Scherrer equation.

XRD results of the ReO_3 NPs are shown in Figure 2(b). The diffraction peaks at $2\theta = 23.7^\circ$ (100), 33.7˚ (110), 41.7˚ (111), 48.5˚ (200), 54.7˚ (210), 60.4˚ (211), 71˚ (220) and 76˚ (300) are consistent with the standard peaks and index for

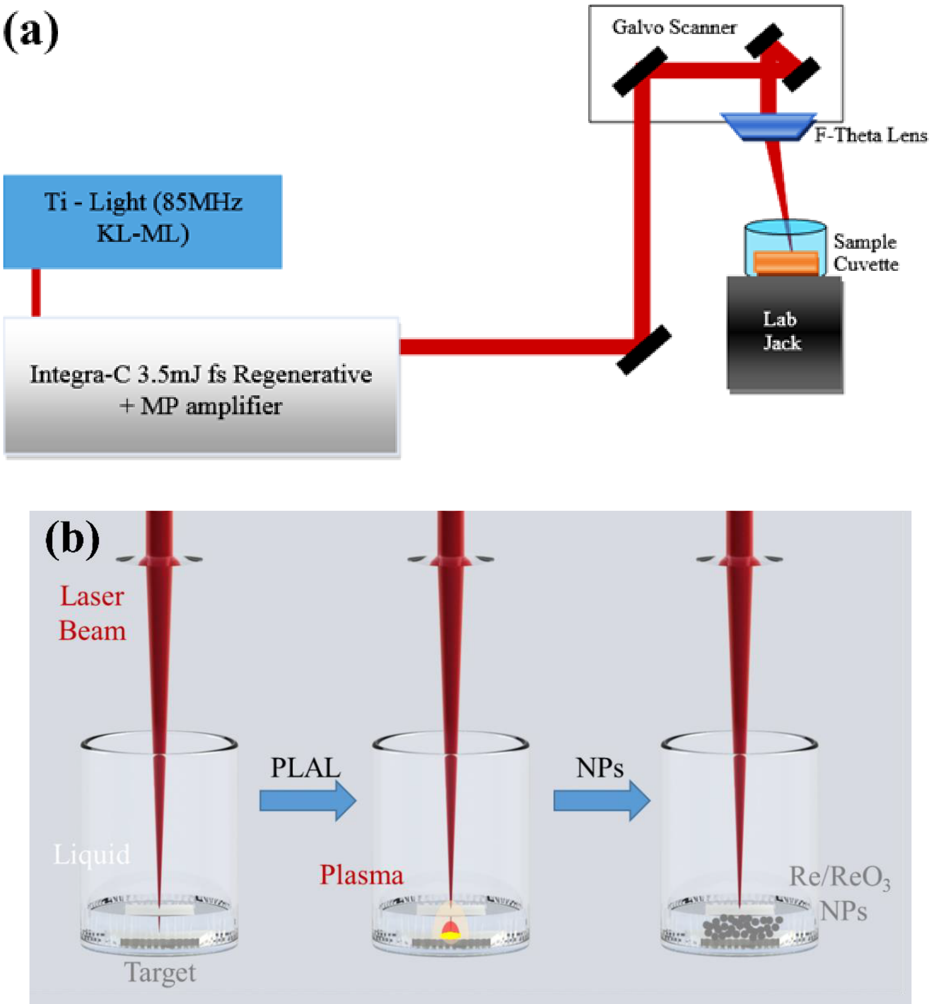

Figure 1. Femtosecond PLAL **(a)** nanoparticle production setup, **(b)** NP production using PLAL method.

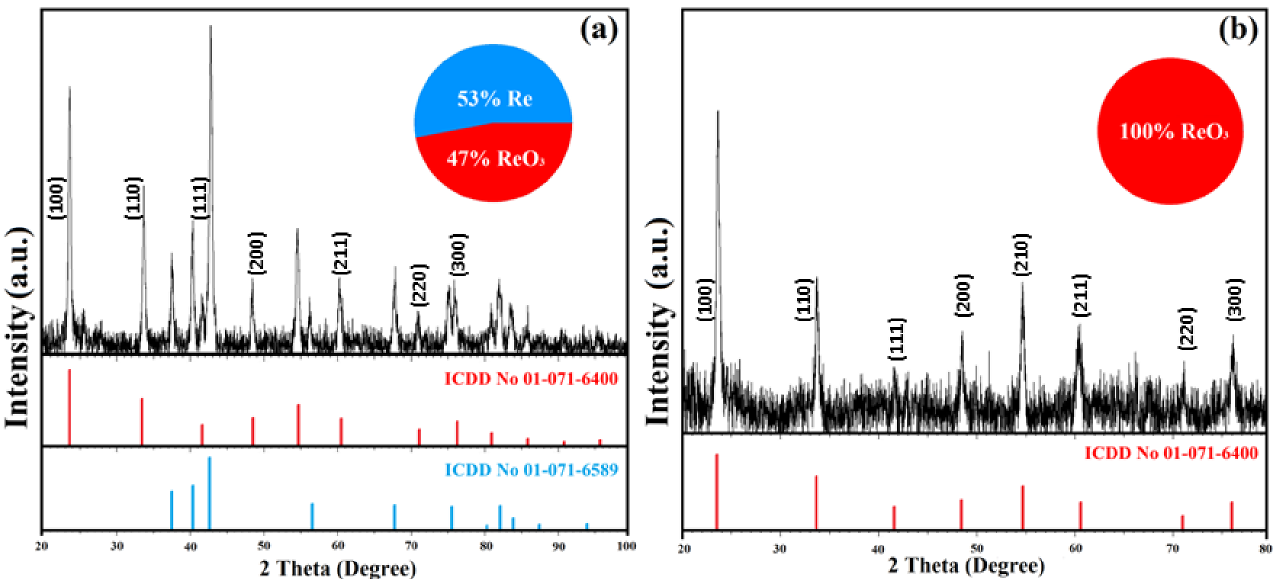

Figure 2. XRD pattern of **(a)** the Re / ReO_3 NPs produced in 30 min, **(b)** ReO_3 NPs were produced in 60 min with low water volume.

ReO_3 in literature [34]. All of the samples show semi-broad diffraction peaks and these broad peaks are due to the small size of the ReO_3 nanocrystals [35]. The average crystallite size of ReO_3 NPs was found to be about 25 nm.

TEM (JEOL JEM-2100F, Japan) and SEM (Zeiss LS 10 - Carl Zeiss NTS GmbH, Germany) analyses have been carried out to present some further properties of the NPs as seen in Figure 3. TEM results of Re / ReO_3 and ReO_3 NPs are given in Figure 3(a) and (d), respectively. According to these results, produced particles have a spherical shape and particle sizes changes from ~ 20 nm (similar to that obtained from XRD crystallite sizes) to ~ 60 nm. Furthermore, HR-TEM analyses

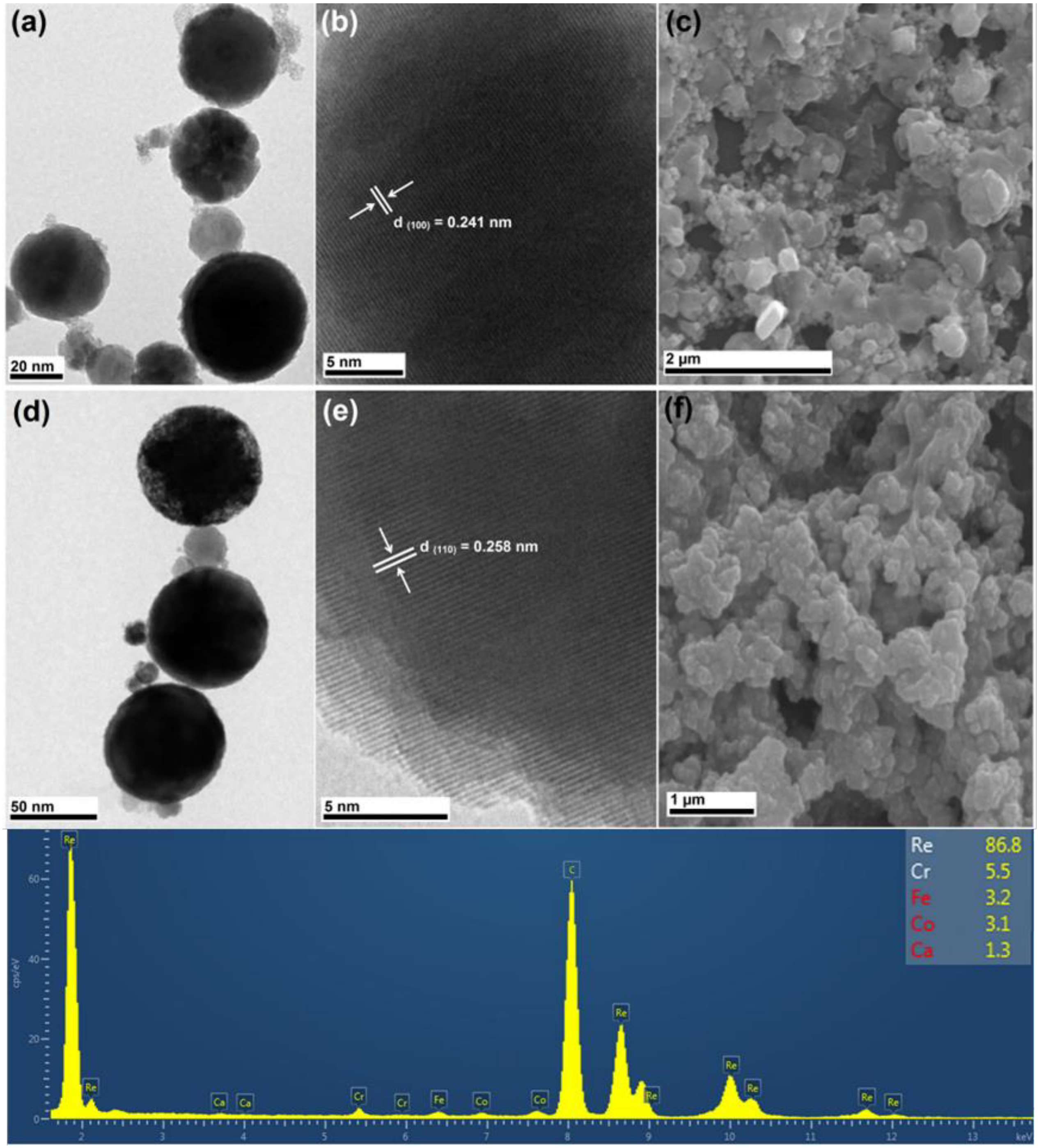

Figure 3. Re / ReO_3 NPs (a) TEM, (b) HR-TEM, (c) SEM images and pure ReO_3 NPs, (d) TEM, (e) HR-TEM, (f) SEM images, and **(g)** EDX Spectra of the NPs show ~86.8% Re, and other metals (Fe, Cr, Co, Ca impurities of the bulk sample) for NP are shown.

were carried out to investigate the crystal structure of Re / ReO_3 and ReO_3 NPs, and these results are given in Figure 3(b) and 3(e). As can be clearly seen from Figure 3(b) and 3(e), atoms constituting the lattice fringes are perfectly arranged and it shows that NPs have highly crystalline nature. The inter-planar spacing of Re and ReO_3 NPs were measured as 5.41 and 2.58 Å, respectively. It is seen that these are due to (100) and (110) crystallographic planes, respectively.

Moreover, samples prepared for SEM imaging were first centrifuged at 1200 rpm for 10 min, NPs were sprinkled to double-sided adhesive band stick on the sample stub and then blow away the loose excessive particles and then samples were coated with gold using sputter coater. SEM images of NPs given in Figure 2(c) and 2(f) show that an increase in duration of the NP production causes solvent evaporation during the sample preparation process and then an increase in the aggregation of NPs. A condensation of the solution after evaporation of the liquid by heating may cause the highly aggregated nanoparticles. Furthermore, as can be seen clearly from Figure 3(c) and 3(f), pure ReO_3 have a homogeneous structure than Re / ReO_3 mixture.

An increase in the sample concentration can cause some increase in the number of photons absorbed by the NPs. This difference in the concentration can also result in an increase in the refractive index of the medium and stronger nonlinear effects like white light continuum (WLC) can be generated [36], and then this may cause some fragmentation of the particles to smaller sized fragments, and therefore, suppresses the aggregation [37]. In this study, in addition to WLC generation, some agglomeration after the end of irradiation was observed dramatically increased in time.

UV-Vis absorption spectra (taken using V-670 spectrometer, Jasco Corp., JAPAN) of Re NPs are given in Figure 4(a) and 4(b). It has been observed that, in the Re / ReO_3 NPs mixture, absorption spectra of Re NPs is dominated by UV-

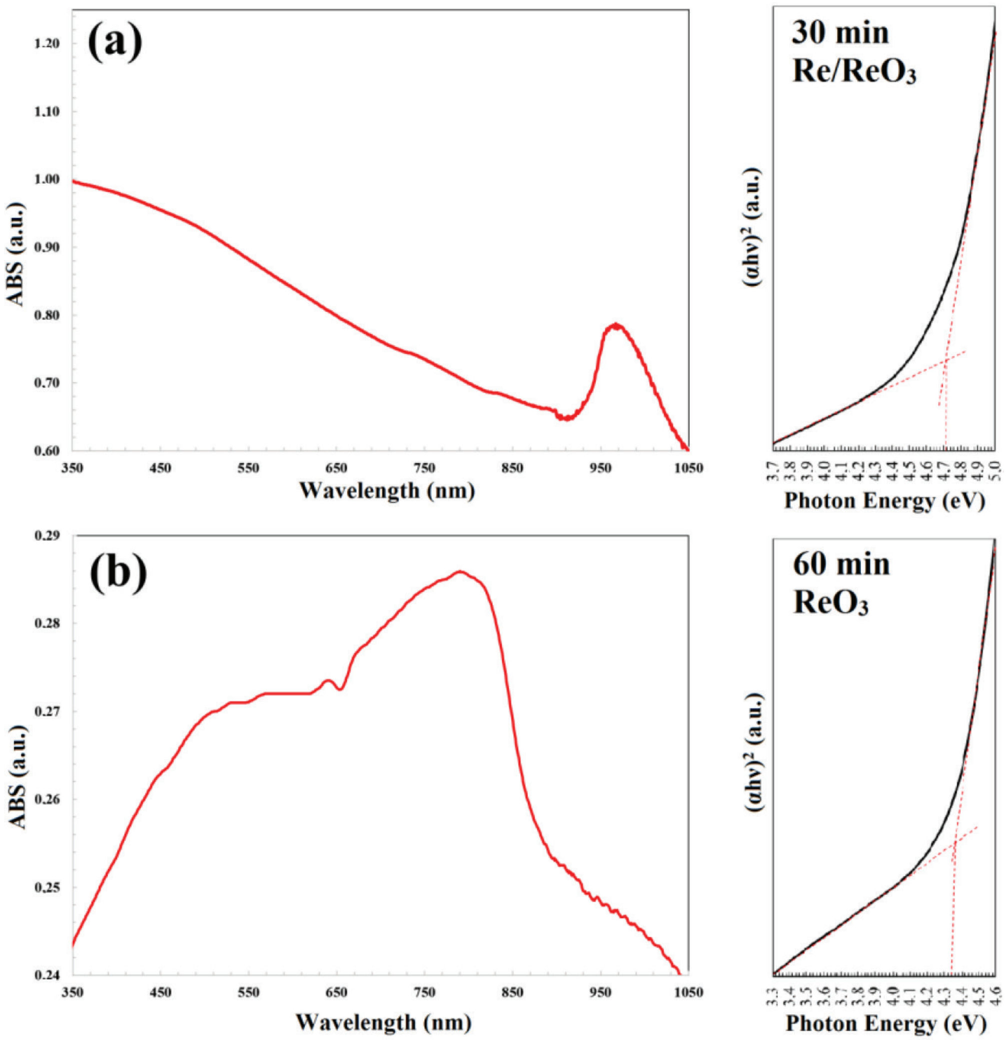

Figure 4. UV-Vis absorption spectra and Tauc-Plots; (a) Re / ReO_3 NPs ablated for 30 min., (b) pure ReO_3.

Vis spectra. The obtained absorption spectrum of the ReO_3 NPs produced in pure water is shown in Figure 4(b), which presents an absorption peak around 510 nm. It has been observed that the obtained absorption peak is compatible with the literature [26].

Band gap values for Re / ReO_3 NPs produced in this work were calculated from the absorption data by using Tauc-plot ($h\nu$–$(\alpha h\nu)^2$) given in Figure 4 [38–40] to be 4.71 eV and 4.36 eV for Re/ReO_3 mixture and pure ReO_3, respectively. It can be concluded that changes in the Tauc-plot indicate that the Re NPs dominates the UV-Vis spectrum. The band gap energy values obtained are also compatible with the literature [34,41,42]. It was found that the absorption spectra of Re/ReO_3 mixture and pure ReO_3 NPs were varied within the range from ultraviolet region to infrared region in spectrum depending on the synthesis parameters.

4. Conclusion

In recent years, rhenium NPs have been used for tumor treating therapies and coatings (plastics, metals, textiles) technologies. In addition, magnetic rhenium NPs have been used as a contrast agent and was produced using both methods of pulsed-laser decomposition of ammonium perrhenate or gamma radiation of dirhenium decacarbonyl.

As a summary, in this study, it has been reported that the Re / ReO_3 NPs mixture or ReO_3 NPs were produced for the first time in the literature using the fsPLAL method. The produced NPs were characterized by XRD, SEM, TEM, EDX, and UV-VIS absorption spectroscopy methods. Re / ReO_3 NP mixtures can also be produced changing laser irradiation time and reducing the liquid volume. Pure ReO_3 NPs can be produced in the high laser fluence regime. XRD results show that pure ReO_3 NPs have perovskite-like cubic structure. Produced particles have a spherical shape and particle sizes change from ~ 20 nm to ~ 60 nm due to the TEM results. SEM results present that micron-sized particles can be aggregated due to the evaporation of the liquid by heating when a large volume of water is used. Wide band gap materials are used in very broad application areas in semiconductor devices, optoelectronic devices, photodetectors, catalytic applications, chemical sensors etc. ReO_3 NPs show a broad absorption band (from 350 nm up to 850 nm), and it can be emphasized that this may indeed be useful for sensors, diodes, and solar cell as photonic applications.

Acknowledgement

Authors kindly thank Selçuk University Scientific Research Projects (BAP) Coordination Unit for financial supports for research projects of 18401178, 19704054 and 19401140.

References

1. Stafe MA, Marcu A, and Puscas NN. Pulsed Laser Ablation of Solids: Basics, Theory and Applications: Springer Science & Business Media; 2013.
2. Yang G, Laser Ablation in Liquids: Principles and Applications in the Preparation of Nanomaterials: CRC Press; 2012.
3. De Bonis A, Lovaglio T, Galasso A, Santagata A, Teghil R. Iron and iron oxide nanoparticles obtained by ultra-short laser ablation in liquid. Applied Surface Science 2015; 353: 433-438. http://dx.doi.org/10.1016/j.apsusc.2015.06.145
4. Chatterjee AK, Sarkar RK, Chattopadhyay AP, Aich P, Chakraborty R et al. A simple robust method for synthesis of metallic copper nanoparticles of high antibacterial potency against E. coli. Nanotechnology 2012; 23 (8): 085103. https://doi.org/10.1088/0957-4484/23/8/085103
5. Awad MA, Hendi AA, Ortashi KM, Elradi DF, Eisa NE et al. Silver nanoparticles biogenic synthesized using an orange peel extract and their use as an anti-bacterial agent. International Journal of Physical Sciences 2014; 9 (3): 34-40. https://doi.org/10.5897/IJPS2013.4080
6. Daniel MC, Astruc D. Gold nanoparticles: assembly, supramolecular chemistry, quantum-size-related properties, and applications toward biology, catalysis, and nanotechnology. Chemical Reviews 2004; 104 (1): 293-346. https://doi.org/10.1021/cr030698
7. El-Sayed, IH, Huang X, El-Sayed M A. Surface plasmon resonance scattering and absorption of anti-EGFR antibody conjugated gold nanoparticles in cancer diagnostics: applications in oral cancer. Nano Letters 2005; 5 (5): 829-834. https://doi.org/10.1021/nl050074e
8. Sperling RA, Gil PR, Zhang F, Zanella M, Parak WJ. Biological applications of gold nanoparticles. Chemical Society Reviews 2008; 37 (9): 1896-1908. https://doi.org/10.1039/B712170A
9. Brust M, Bethell D, Kiely CJ, Schiffrin DJ. Self-assembled gold nanoparticle thin films with nonmetallic optical and electronic properties. Langmuir 1998; 14 (19): 5425-5429. https://doi.org/10.1021/la980557g
10. Ung T, Liz-Marzan LM, Mulvaney P. Gold nanoparticle thin films. Colloids and Surfaces A: Physicochemical and Engineering Aspects 2002; 202 (2): 119-126. https://doi.org/10.1016/S0927-7757(01)01083-4

11. Ouyang J, Chu C-W, Szmanda CR, Ma L, Yang Y. Programmable polymer thin film and non-volatile memory device. Nature Materials, 2004; 3 (12): 918-922. https://doi.org/10.1038/nmat1269

12. Kim YL, Choi H-A, Lee N-S, Son B, Kim HJ et al. RuO 2–ReO 3 composite nanofibers for efficient electrocatalytic responses. Physical Chemistry Chemical Physics 2015; 17 (11): 7435-7442. https://doi.org/10.1039/C4CP05615A

13. Yoo S-J, Chang J-H, Lee J-H, Moon C-K, Wu C-I, et al. Formation of perfect ohmic contact at indium tin oxide/N, N [prime]-di (naphthalene-1-yl)-N, N [prime]-diphenyl-benzidine interface using ReO3. Scientific Reports 2014; 4. https://doi.org/10.1038/srep03902

14. Karan HI, Sasaki K, Kuttiyiel K, Farberow CA, Mavrikakis M et al. Catalytic activity of platinum monolayer on iridium and rhenium alloy nanoparticles for the oxygen reduction reaction. ACS Catalysis 2012; 2 (5): 817-824. https://doi.org/10.1021/cs200592x

15. Taratanov N, Yurkov GY, Koksharov YA, Bouznik V. Preparation and properties of composite materials based on rhenium-containing nanoparticles and micrograins of polytetrafluoroethylene. Inorganic Materials: Applied Research 2011; 2 (2): 118-124. https://doi.org/10.1134/S2075113311020201

16. Ghosh S, Biswas K, Rao C. Core–shell nanoparticles based on an oxide metal: ReO 3@ Au (Ag) and ReO 3@ SiO 2 (TiO 2). Journal of Materials Chemistry 2007; 17 (23): 2412-2417. https://doi.org/10.1039/B701137G

17. Chong, Y.Y., W.Y. Chow, and W.Y. Fan, Preparation of rhenium nanoparticles via pulsed-laser decomposition and catalytic studies. Journal of Colloid and Interface Science 2012; 369 (1):164-169. https://doi.org/10.1016/j.jcis.2011.12.015

18. Ayvalı T, Lecante P, Fazzini P-F, Gillet A, Philippot K et al. Facile synthesis of ultra-small rhenium nanoparticles. Chemical Communications 2014; 50 (74): 10809-10811. https://doi.org/10.1039/C4CC04816D

19. Bedia J, Calvo L, Lemus J, Quintanilla A, Casas JA et al. Colloidal and microemulsion synthesis of rhenium nanoparticles in aqueous medium. Colloids and Surfaces a-Physicochemical and Engineering Aspects 2015; 469: 202-210. https://doi.org/10.1016/j.colsurfa.2015.01.031

20. Zinn AA. Inventor; Google Patents, assignee. Rhenium Nanoparticles 2010.

21. Rojas J, Castano CH. Synthesis of rhenium oxide nanoparticles (Re x O y) by gamma irradiation. Radiation Physics and Chemistry 2014; 99: 1-5. https://doi.org/10.1016/j.radphyschem.2014.01.022

22. Tang N, Tu W. Synthesis of magnetic rhenium sulfide composite nanoparticles. Journal of Magnetism and Magnetic Materials 2009; 321 (19): 3311-3317. https://doi.org/10.1016/j.jmmm.2009.06.049

23. Tu W, Denizot B. Synthesis of small-sized rhenium sulfide colloidal nanoparticles. Journal of Colloid and Interface Science 2007; 310 (1): 167-170. https://doi.org/10.1016/j.jcis.2007.01.054

24. Ohkubo M, Fukai K, Kohji M, Iwata N, Yamamoto H. Preparation of conductive ReO3 thin films. Superconductor Science and Technology 2002; 15 (12): 1778. https://doi.org/10.1088/0953-2048/15/12/332

25. Pearsall T, Lee C. Electronic transport in Re O 3: dc conductivity and Hall effect. Physical Review B 1974; 10 (6): 2190. https://doi.org/10.1103/PhysRevB.10.2190

26. Biswas K, Rao C. Metallic ReO3 nanoparticles. The Journal of Physical Chemistry B 2006; 110 (2): 842-845. https://doi.org/10.1021/jp055670b

27. Mocatta D, Cohen G, Schattner J, Millo O, Rabani E et al. Heavily doped semiconductor nanocrystal quantum dots. Science 2011; 332 (6025): 77-81. 10.1126/science.1196321

28. Kim J-B, Lee J-H, Moon C-K, Kim J-J. Highly efficient inverted top emitting organic light emitting diodes using a transparent top electrode with color stability on viewing angle. Applied Physics Letters 2014; 104 (7): 073301. https://doi.org/10.1063/1.4865765

29. Gündoğdu Y, Kepceoğlu A, Gezgin SY, Küçükçelebi H, Kılıç HŞ. Femtosecond laser ablation synthesis of nanoparticles and nano-hybrides in ethanol medium. Materials Today: Proceedings 2019; 18: 1803-1810. https://doi.org/10.1016/j.matpr.2019.06.667

30. Zhigilei LV, Lin Z, Ivanov DS. Atomistic modeling of short pulse laser ablation of metals: connections between melting, spallation, and phase explosion. The Journal of Physical Chemistry C 2009; 113 (27): 11892-11906. https://doi.org/10.1021/jp902294m

31. Salminen T. Production of nanomaterials by pulsed laser ablation. Tampereen teknillinen yliopisto. Julkaisu-Tampere University of Technology 2013.

32. Jørgensen J-E, Jorgensen J, Batlogg B, Remeika J, Axe J. Order parameter and critical exponent for the pressure-induced phase transitions in ReO3. Physical Review B 1986; 33: 4793-4798. https://doi.org/10.1103/PhysRevB.33.4793

33. Holzwarth U, Gibson N. The Scherrer equation versus the 'Debye-Scherrer equation'. Nature Nanotechnology 2011; 6 (9): 534-534. https://doi.org/10.1038/nnano.2011.145

34. Jeong Y-K, Lee Y M, Yun J, Mazur T, Kim M et al. Tunable photoluminescence across the visible spectrum and photocatalytic activity of mixed-valence rhenium oxide nanoparticles. Journal of the American Chemical Society 2017; 139 (42): 15088-15093. https://doi.org/10.1021/jacs.7b07494

35. Ghosh S, Lu HC, Cho SH, Maruvada T, Price MC et al. Colloidal ReO3 nanocrystals: extra re d-electron instigating a plasmonic response. Journal of the American Chemical Society 2019; 141 (41): 16331-16343. https://doi.org/10.1021/jacs.9b06938

36. Liu W, Kosareva O, Golubtsov IS, Iwasaki A, Becker A et al. Femtosecond laser pulse filamentation versus optical breakdown in H2O. Applied Physics B 2003; 76 (3): 215-229. https://doi.org/10.1007/s00340-002-1087-1

37. Besner S, Kabashin AV, Winnik FM, Meunier M. Synthesis of size-tunable polymer-protected gold nanoparticles by femtosecond laser-based ablation and seed growth. The Journal of Physical Chemistry C 2009; 113 (22): 9526-9531. https://doi.org/10.1021/jp809275v

38. Tauc J, Grigorovici R and Vancu A. Optical properties and electronic structure of amorphous germanium. Physica Status Solidi (b) 1966; 15 (2): 627-637. https://doi.org/10.1002/pssb.19660150224

39. Yıldırım M, Özel F, Sarılmaz A, Aljabour A, Patır İH. Investigation of structural, optical and dielectrical properties of Cu2WS4 thin film. Journal of Materials Science: Materials in Electronics 2017; 28 (9): 6712-6721. 10.1007/s10854-017-6365-0

40. Yıldırım M, Aljabour A, Sarılmaz A, Özel F. Investigation of optical framework of chalcostibite nanocrystal thin films: An insight into refractive index dispersion, optical band gap and single-oscillator parameters. Journal of Alloys and Compounds 2017; 722: 420-426. https://doi.org/10.1016/j.jallcom.2017.06.157

41. Kundu S, Ma L, Dai W, Chen Y, Sinyukov A M et al. Polymer encapsulated self-assemblies of ultrasmall rhenium nanoparticles: catalysis and SERS applications. ACS Sustainable Chemistry & Engineering 2017; 5 (11): 10186-10198. https://doi.org/10.1021/acssuschemeng.7b02175

42. Revina A, Kuznetsov MA, Chekmarev AM, Boyakov EE, Zolotarevskii V. Synthesis and physicochemical properties of rhenium nanoparticles. Protection of Metals and Physical Chemistry of Surfaces 2018; 54 (1): 43-50. https://doi.org/10.1134/S2070205118010112